ARTICLE OPEN

Entangling motional atoms and an optical loop at ambient condition

Xiao-Ling Pang[1,2,5], Chao-Ni Zhang[1,2,5], Jian-Peng Dou[1,2,5], Hang Li[1,2], Tian-Huai Yang[1,2] and Xian-Min Jin[1,2,3,4]✉

The observation of quantum entanglement in macroscopic matters has implications in the fundamental studies of quantum mechanics, as well as the implementations of quantum information technologies, such as quantum communication, enhanced sensing, and distributed quantum computing. Here, we report the creation of the heralded entanglement between two different room-temperature quantum memories: a single-photon entangled state delocalized between motional atoms as a collective excitation and an all-optical loop as a flying qubit. The stored entangled state is subsequently retrieved and verified by measuring the nonclassical correlations, quantum interference, and concurrence of the mapped-out photons. Our results show that quantum entanglement can be sustained in macroscopic matters at ambient condition, which enriches the fundamental researches of the transition boundary between quantum and classical worlds. Also, it highlights the potential cooperation between atomic ensembles and all-optical loop as quantum nodes at ambient condition, bringing a significant step towards practical quantum networks.

npj Quantum Information (2023)9:62 ; https://doi.org/10.1038/s41534-023-00715-7

INTRODUCTION

Human perception of the real-life world is mainly derived from the phenomena of macroscopic matter movements, described by the laws of classical physics. Quantum mechanics, however, endows the nature of superposition and entanglement is able to express the universe in a clearer and more concise manner. Therefore, expanding quantum theory to more general ambient systems and exploring the quantum phenomena in macroscopic objects push the researches of the transition boundary between classical and quantum realm[1,2]. On the other hand, the capability of establishing and sharing remote high-fidelity entanglement over long distances is necessary for scalable quantum technologies which promise to outperform their classical counterparts, such as in the areas of communication, computing, sensing, and metrology[3–12].

Over the past two decades, enormous advances have been made in entangling macroscopic systems, and quantum entanglement has been observed in some matter systems, such as atomic ensembles[5,13–17], individual atoms[18], trapped ions[19], quantum dots[20], color centers[21–25], and massive mechanical oscillators[2,26]. While, due to strong internal interactions and external coupling with the environment, it is still challenging to observe quantum entanglement with a low noise level in macroscopic systems at ambient condition. Photons, as the most widely-used state carriers in quantum world today, still suffer from inevitable loss, either propagating in free space or optical fibers[27,28]. Together with the probabilistic nature of quantum mechanics[29,30], the creation and dissemination of the entangled states are hard to scalable for longer distances or for more nodes in a quantum network.

Quantum-memory-assisted repeaters provide an elegant solution, with which the heralded remote entanglement can be stored and retrieved on demand[31–41], enabling a polynomial increase rather than an exponential growth in time consumption in a network. Practical applications of scalable quantum memories require some advantageous features, such as high efficiency, long lifetime, low noise level, wavelength compatibility, storable number of modes, and operable at high bandwidth[42]. In addition, though troubled by the harmful decoherence and noise, operating with room-temperature systems has been attractive since its simpler operation requirement, especially in the case where many memory units are involved. Such quantum-memory-enabled networks are pursued for generating, storing, processing, and disseminating heralded entanglement, in real-life quantum information technologies, overcoming the most critical barriers including photon loss and probabilistic sources.

In this paper, we study the creation and retrieval of the collective excitation state in motional atoms and the broadband storage of the loop architecture. Such two memory-built-in quantum nodes constitute a hybrid quantum network at ambient condition. Based on the implementations, we observe the heralded quantum entanglement between motional atoms and an optical loop located on separated platforms at room temperature. The coherence time of both quantum memories is all at microsecond level, which is demonstrated in our previous work[43]. To reveal the quantum entanglement, the states stored in these two quantum memories are mapped back to optical modes, then via a single-photon interference, we obtain the concurrence and density matrix of the retrieved light modes. We also observe a violation of Cauchy–Schwarz inequality[44] up to 209 SDs, which implies that the nonclassical feature of the photons is demonstrated with high confidence. A cross-correlation value up to 15.39 ± 0.26 well exceeds the boundary of 6 above which quantum correlation is able to violate Bell's inequality[45,46], and this promises further quantum applications.

[1]Center for Integrated Quantum Information Technologies (IQIT), School of Physics and Astronomy and State Key Laboratory of Advanced Optical Communication Systems and Networks, Shanghai Jiao Tong University, Shanghai 200240, China. [2]Hefei National Laboratory, Hefei 230088, China. [3]TuringQ Co., Ltd., Shanghai 200240, China. [4]Chip Hub for Integrated Photonics Xplore (CHIPX), Shanghai Jiao Tong University, Wuxi 214000, China. [5]These authors contributed equally: Xiao-Ling Pang, Chao-Ni Zhang, Jian-Peng Dou. ✉email: xianmin.jin@sjtu.edu.cn

RESULTS

Creating the heralded entanglement between two quantum memories

The experimental scheme used for generating photons is based on the far-off-resonance Duan–Lukin–Cirac–Zoller protocol in a memory-built-in fashion, and its implementations have been demonstrated as intrinsically broadband and low-noise at room temperature[43,47,48]. As is shown in Fig. 1, initially, motional atoms are prepared into the ground state $|g\rangle$, waiting for the write pulse to produce an excitation among atoms, and meanwhile, the process is accompanied by a flying Stokes photon via spontaneous Raman scattering to herald a successful creation of an excitation. After a programmable storage time, the collective excitation state can be mapped out as an anti-Stokes photon, and into various temporal modes by a series of read pulse. The probability distribution can be tuned by applying different amplitudes of each read pulse.

An all-optical loop serves as another quantum memory node, for mapping flying anti-Stokes modes in and out with programmable storage times individually. Once a Stokes photon occurs, the horizontally-polarized anti-Stokes mode entering the loop will be converted to vertically-polarized, so that the photon will be trapped in the optical loop until its polarization is converted back.

The entanglement is established by applying the first read pulse on atoms, and the collective excited state is converted back to anti-Stokes photons with a tunable retrieval efficiency. By sending this retrieved anti-Stokes mode A to the all-optical loop, the detection of a Stokes photon at D_S heralds the creation of a single excitation delocalized between the two quantum memories, and the entangled state can be sustained until the second read pulse is applied to atoms for retrieving the state. Notably, the generated atom-photon pair in the write process is actually in a two-mode-squeezed state, implying the existence of vacuum and high-order excitation terms during this process. Here we apply a quite weak write pulse so that the probability of high-order excitation term is extremely small, and it can be neglected in this case. Therefore, when registering a Stokes photon in the detector, we can assume that a collective excitation is created in the atomic ensemble after the write process, and the established entangled state now can be written as:

$$|\Psi_{\text{Joint}}\rangle = (\alpha|1\rangle_{\text{Loop}}|0\rangle_{\text{Atoms}} + \beta e^{i\gamma}|0\rangle_{\text{Loop}}|1\rangle_{\text{Atoms}})/\sqrt{2} \quad (1)$$

where $|1\rangle_{\text{Atoms}}$ represents a collective excitation state[49] in the atomic ensemble, and $|1\rangle_{\text{Loop}}$ represents an anti-Stokes photon trapped in the optical loop. The value of α and β are configurable by applying various pulse energy of the retrieval light. The phase difference γ is dependent on the generation time and propagation paths of two readout modes. The phase jitter of γ is caused by the optical loop which is the only difference of the propagation paths of these two modes, and can be suppressed by the phase locking circuit shown in Fig. 2.

In our experiment, two read pulses are applied for retrieving the stored excitation state, and the energy of each read pulse is finely tuned to obtain the approximately same retrieval efficiency (see Methods for details), so that a maximumally entangled state can be created. Once a Stokes photon is detected, the excitation will be mapped out into two temporal modes (denoted by mode A at $t1$ and mode B at $t2$) with the same probability, as a single-photon entangled state $(|1\rangle_{t1}|0\rangle_{t2} + |0\rangle_{t1}|1\rangle_{t2})/\sqrt{2}$. We will be able to read the entangled state by programing the storage time of both quantum memories in a coordinated fashion. Experimental setup and time sequences of the control and pump pulses are illustrated in Fig. 2.

The verification of the entanglement

Observing a strike at detector D_S, therefore, heralds the presence of the entanglement between two quantum memories with a predictable time delay. To reveal the quantum entanglement, the second incident read pulse is applied to convert the excitation state in motional atoms to optical mode, meanwhile, a read signal is applied to map out the flying photon in the optical loop by

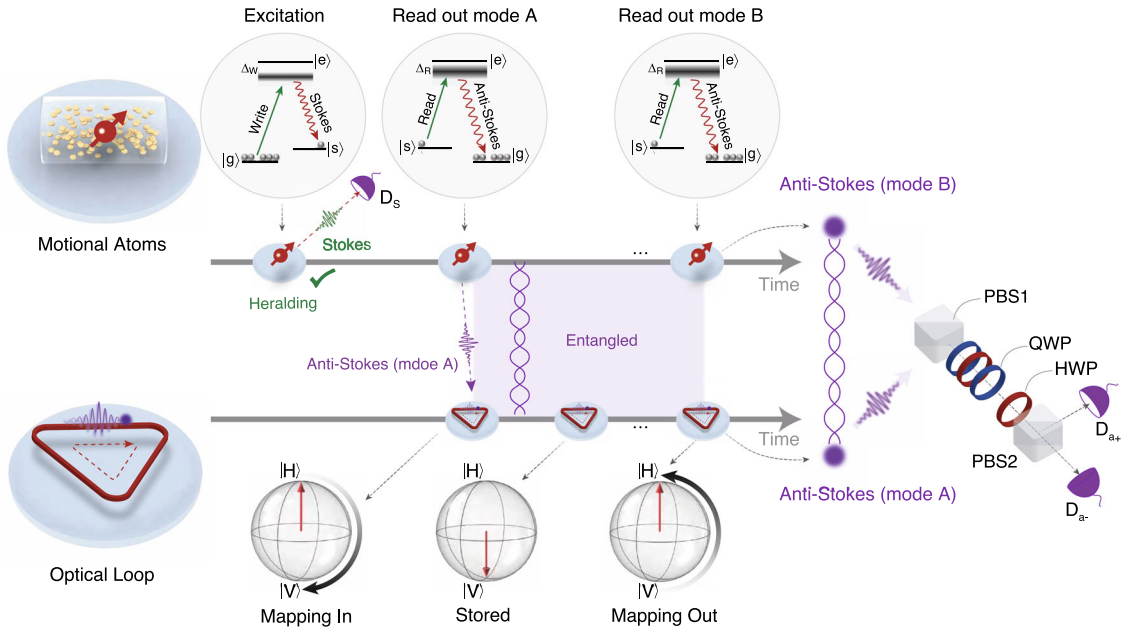

Fig. 1 Schematic of establishing and verifying the hybrid entanglement between an optical loop and motional atoms. The generation of photons, and the creation, storage, and verification of entanglement are illustrated from the left to right. The insets above describe write and read processes of the far-off-resonance Duan–Lukin–Cirac–Zoller protocol, with the three-level Λ-type configuration of atoms. $|g\rangle$ and $|s\rangle$ represent hyperfine ground states. Insets below describe the polarization states of the optical modes, shown in Bloch spheres. The first polarization beam splitter (PBS1) combines the retrieved two optical modes, and the following half-wave plate (HWP) and two quarter-wave plates (QWP) rotate and mix the fields, resulting the single-photon interference on a polarization beam splitter (PBS). $D_{S/a}$ Detector of Stokes/anti-Stokes photons.

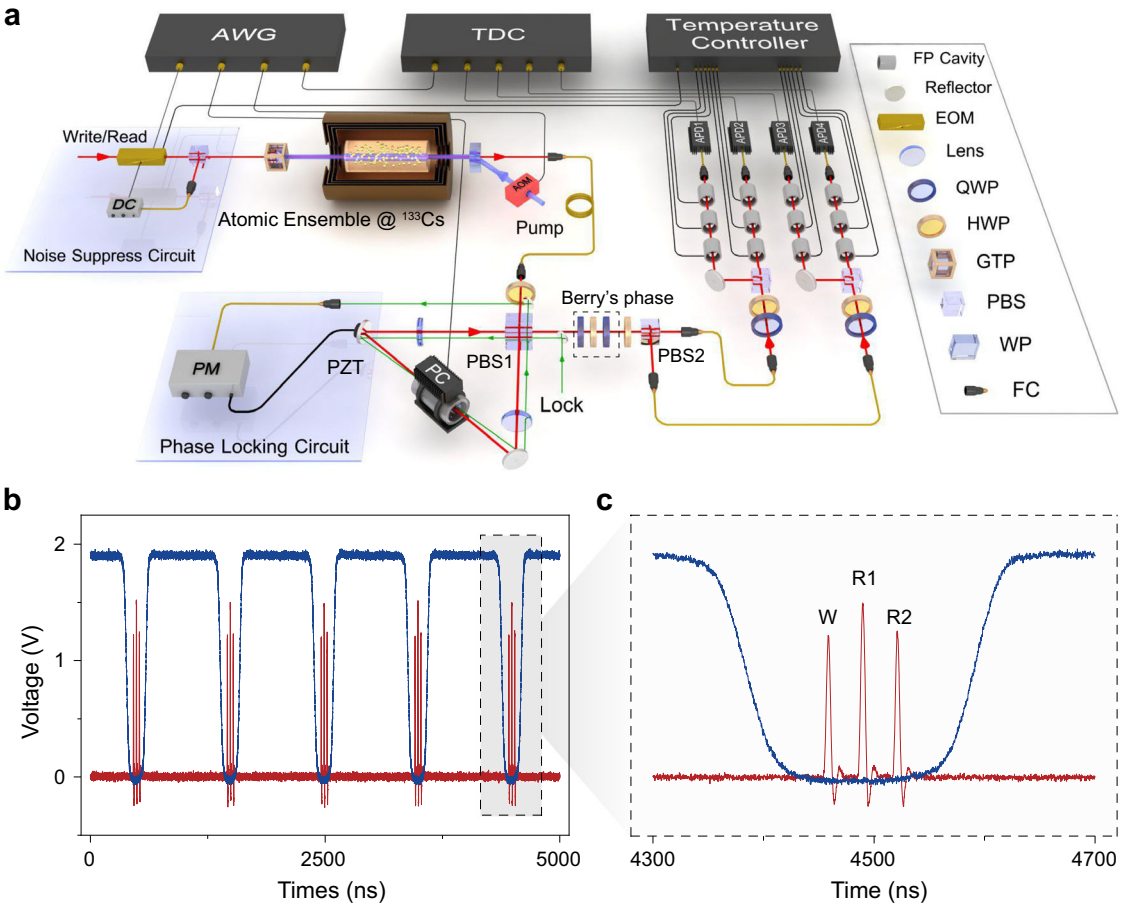

Fig. 2 Experimental schemes. a Experimental setups. The manipulation of the Pancharatnam and Berry's phase is realized by a combination of QWP-HWP-QWP elements. The two QWPs are set at 45°, and 10° rotation of the HWP brings 40 degrees phase added in two anti-Stokes modes. AWG arbitrary waveform generator, TDC time-to-digital converter, EOM electro-optic modulator, HWP half-wave plate, QWP quarter-wave plate, GTP Glan-Taylor prism, PBS polarization beam splitter, WP Wollaston prism, PZT piezoelectric ceramics, AOM acousto-optical modulators, FC fiber coupler, PC Pockels cells, DC direct-current controlller, PM phase modulator, APD avalanche photodiode. The detectors APD2 and APD4 detect the generated Stokes photons while the detectors APD1 and APD3 register the generated anti-Stokes photons. **b** Time sequences of the control pulses (red lines) and pump pulses (blue lines). **c** A magnification view of the time sequences where the interval between two read pulses is set as 30 ns.

converting its polarization state back to horizontal. Therefore, the entanglement between two quantum memories is mapped to the entanglement between two anti-Stokes modes, which are then combined on a polarizing beam splitter.

After an extra-added controllable Pancharatnam-Berry's phase[50] outside the all-optical loop, two modes interfere on a half-wave plate and the following polarizing beam splitter. The interference can be observed by tuning the Pancharatnam-Berry's phase, and the projected results of the retrieved single photon delocalized in two memories are recorded by the detectors after two ports N_+ and N_-, shown in Fig. 3. We observe the single-photon interference curve, and the calculated visibility value up to $(88 \pm 5)\%$ indicates that the coherence between two stored modes is preserved well during the storage time of 60 ns. Note that the phase difference induced by environment fluctuation between two optical modes in our experiment is rigorously stabilized by a beam of continuous wave light (phase-locking light) and a feedback circuit equipped with piezoelectric ceramics. In addition, the extra-added controllable Pancharatnam-Berry's phase we introduce here is free of the phase-locking process, making it possible to control the phase arbitrarily. Details can be found in "Methods".

The second-order correlation function $g^{(2)}_{S-AS}$ evaluates the performance of the systems to preserve quantum correlations. We therefore measure the second-order correlation functions between the heralding Stokes photons and the retrieved anti-Stokes modes after transmitting through the whole system, coming up to 15.39 ± 0.26. A violation of Cauchy–Schwarz inequality $\left(g^{(2)}_{S-AS}\right)^2 \leq g^{(2)}_{S-S} \cdot g^{(2)}_{AS-AS}$[44] after the whole hybrid system is also observed as 209 SDs ($g^{(2)}_{S-S} = 1.72 \pm 0.12$ and $g^{(2)}_{AS-AS} = 1.56 \pm 0.26$), which indicates a high-fidelity generation and preservation of non-classical correlation at ambient conditions.

The joint state of the retrieved anti-Stokes modes is described by a density matrix ρ in the Fork state basis, in which the entanglement can be revealed by a tomographic approach[13,51,52]. According to the measurement results of the correlated photons, the density matrix can be deduced in the form in Fig. 4. The heralded probabilities of p_{mn} represent the registration of m photons in mode A, and n photons in mode B, conditioned on a detected Stokes photons, $\{m, n\} = \{0, 1\}$. The off-diagonal terms represent coherence $d = V(p_{01} + p_{10})/2$, and V is the visibility of interfering two heralded anti-Stokes modes obtained previously. Higher-order photon numbers are ignored. The concurrence of the density matrix ρ, therefore, is given by[13,53]

$$C = \max(0, V(p_{01} + p_{10}) - 2\sqrt{p_{00}p_{11}}) \quad (2)$$

A non-zero concurrence indicates the entangled state, while a zero concurrence indicates separable state. To maximize the

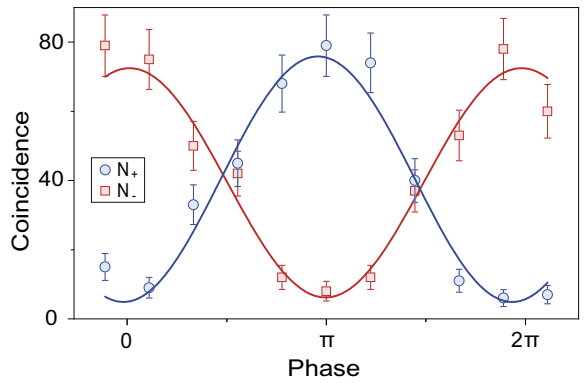

Fig. 3 Coincidence counts between heralding Stokes photons and mapped out anti-Stokes photons. The visibility is measured up to (88 ± 5)% for N_+ and (84 ± 6)% for N_-. The repetition rate of the experimental trials is 1 MHz and the total count time is 1 h, thus the total number of trials is 3.6×10^9 for obtaining one data point. Error bars are derived by Poisson distribution of avalanched photodiodes.

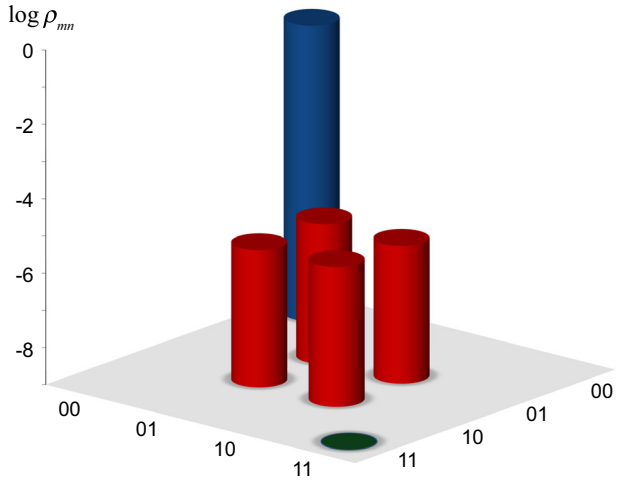

Fig. 4 The reconstructed density matrix of the two retrieved anti-Stokes modes. Elements are $p_{00} = 1 - 4.00 \times 10^{-4}$, $p_{01} = (2.03 \pm 0.07) \times 10^{-4}$, $p_{10} = (1.97 \pm 0.06) \times 10^{-4}$, $p_{11} = (1.11 \pm 0.05) \times 10^{-8}$, $d = (1.72 \pm 0.09) \times 10^{-4}$. The diagonal terms are measured with no interference between two anti-Stokes modes, and p_{11} indicates the probability of higher-order events, which is much smaller than that of single excitation.

concurrence, from equation (2), one may increase the probabilities of detecting heralded states (p_{01}, p_{10}), and decrease the probabilities of detecting the separable states $|0\rangle|0\rangle$ (p_{00}) and $|1\rangle|1\rangle$ (p_{11}), as well as improve the interference visibility (V). We calculate the concurrence in our system to be $(1.33 \pm 0.18) \times 10^{-4}$, which is on the same order of magnitude as the maximum value ($C_{max} = 4.00 \times 10^{-4}$, when $V = 1$ and $p_{11} = 0$), here the p_{11} is calculated according to the cross-correlation value with the relationship of $p_{11} = 4p_{10}p_{01}/(g^{(2)}_{S-AS} - 1)$[54] based on the assumption that the Duan–Lukin–Cirac–Zoller light source generates a two-mode-squeezed state[49]. Since local process cannot increase the entanglement, our measurement gives a lower bound for the entanglement between two quantum memories. Note that the maximum concurrence is limited by the efficiency of the whole system, including retrieval, coupling, and detecting efficiencies for the anti-Stokes photons. The retrieval efficiency for the anti-Stokes photons can be further improved in our experiment by introducing individual control of the write and read lasers, employing higher transmittance optical elements, or applying other available protocols.

Since the two retrieved anti-Stokes modes are all vertically polarized when entering the optical loop, to map the first-arrived mode into the loop, a half-wave plate set at 22.5° is placed just before the optical loop, as is shown in Fig. 2. Then we map the horizontally polarized component of the first mode into the loop, and after programmable storage, it is retrieved and combined with the vertically polarized component of the second mode on PBS1 in both time and space domain. Alternatively, the half-wave plate can be replaced by a high-speed electrooptical modulator, so that the certain anti-Stokes modes can be selected with a doubled efficiency.

DISCUSSION

For the optical loop memory, the limitation of storage efficiency and lifetime is set by the transmission efficiency of the Pockels cell. The Pockels cell with a higher transmission efficiency and a higher bandwidth is about to be upgraded. For the DLCZ memory based on warm atoms, the dominant factor of decoherence mechanism is random motion-induced loss of atoms. By keeping atoms staying in the interaction region, applying a small-diameter cell is an available way to alleviate the above detrimental effect for longer memory lifetime[55,56]. In addition, anti-relaxation coating should be adopted to preserve the atomic polarization during the collision between atoms and the inner wall of glass cell. Besides, it is promising to prolong the storage time of quantum memory by transferring the spin-wave of alkaline metal atoms to noble-gas nuclear spins in the regime of spin exchanging, as is proposed in ref. [57].

In summary, we herald a hybrid quantum entanglement between two different types of broadband quantum memories located on separated platforms at ambient condition, and reveal the entangled state between an all-optical loop and motional atoms. The measured high cross-correlation values between Stokes and anti-Stokes photons identify the capability of quantum memories to preserve quantum correlations, and the single-photon interference visibility and concurrence between two heralded anti-Stokes modes exhibit that the entangled state is protected well during the storage time.

Quantum entanglement built and observed in such macroscopic hybrid matters is profound for the fundamental researches of exploring both quantum and classical worlds, or more specifically, it pushes the transition boundary from quantum to classical. For real-life applications, arbitrary qubit could be teleported to the all-optical loop or warm atoms. Also, quantum repeaters based on memories could be built for quantum communications, which promises for scalable and high-speed quantum networks. More importantly, the large time-bandwidth product and the ability to operate at ambient condition of both quantum memories make the network promptly applicable.

METHODS

Experimental details

We use cesium atoms ^{133}Cs to achieve a large optical depth due to its higher saturated vapor pressure compared with other alkali atoms. The 75-mm-long cesium cell with 10 torr Ne buffer gas is placed into a magnetic shielding and is heated up to 61° centigrade to obtain an optical depth of about 5000. The width of the control pulses in our far-off-resonance Duan–Lukin–Cirac–Zoller protocol is around 4 ns, and the corresponding storage bandwidth is 300 MHz calculated by utilizing the convolution theorem and Fourier transform[58]. In our experiment, we develop a programmable and high-intensity light pulse generation system to create control pulses. The output frequency of the laser diode is

locked to the transition $6S_{1/2}, F = 4$ to $6S_{3/2}, F' = 4$ co 5 line of cesium, with 4 GHz detuning.

Then a high-speed (10 GHz) waveguide electrooptical modulator is applied to chop the continuous laser into short pulses. Combined with an arbitrary waveform generator (2.4 GHz bandwidth), we can finely tune both the shape and energy of the control light sequences. The working temperature of the electrooptical modulator is locked by a temperature controller, and a feedback circuit on its bias voltage is also added to minimize the real-time background noise by monitoring the modulated light signals. After amplifying and filtering, the signal-to-noise ratio of the pulse light reaches 200:1. By using a power meter, we obtain the pulse energy of the write pulse, the first read pulse, and the second read pulse are 370 pJ, 521 pJ, and 373 pJ, respectively, and in this case, the amplitudes of the two retrieved anti-Stokes modes after the whole system are approximately the same. The beam waist is measured as 360 μm.

The maximum total transmission efficiency of the cascaded FP cavity filters is about 70%. Based on the spectra of the photons and the bandwidth (380 MHz) of cascaded FP cavity filters, we can calculate the practical transmission efficiency of the cascaded cavity filters is about 50%. The transmission efficiency of the Pockels cell in the optical loop is about 85%. The rise/fall time of the Pockels cell is 6 ns. The storage efficiency of the loop memory is about 80% for a short storage time 10 ns. That is there is 20% loss after the photons propagate one round in the optical loop, and 50% loss after three rounds in the loop. The total transmission efficiency of the light from the DLCZ quantum memory to the single-photon detectors is about 0.4% for Stokes photons and anti-Stokes photons mode B while the overall transmission efficiency for anti-Stokes photons mode A is 0.2%. There are actually many fiber collimators, fiber flanges, which result in very low total transmission efficiency. The detection efficiency of single-photon detectors is about 50%. Thus, the total efficiency is about 0.2% for Stokes photons and anti-Stokes photons mode B while this efficiency is 0.1% for anti-Stokes photons mode A.

Locking an unbalanced interferometer

The interference in our implementation is realized with an unbalanced interferometer of 9-m-length difference. To observe a high visibility interference, the impact of environmental noise should be eliminated rigorously. Thus as is indicated in Fig. 2, another beam of auxiliary phase-locking light is injected into the optical loop to stabilize the phase jitter induced by temperature drift and other mechanical vibrations in the ambient. Note that such phase-locking light has to satisfy that its coherence time is much longer than the unbalanced length of interferometer, as well as that its frequency jitter is negligible. Therefore, we utilize the same laser source with the signal photons (part of the control light), to minimized the phase difference caused by the frequency jitter of the laser sources. The frequency of the control light (also the phase-locking light) is locked to the transition $6S_{1/2}, F = 4$ to $6S_{3/2}, F' = 4$ co 5 line of ceasium, with 4 GHz detuning.

The phase-locking light and the signal photons are set to be parallel but not collinear, with opposite directions to avoid introducing noise photons. A piezoelectric ceramics is mounted on one of the reflectors in the optical loop, cooperating with the photodetector and voltage source, to form a feedback circuit. The interference of classical phase-locking light detected by the photodetector is then modulated, demodulated, and after passing through a low-pass electrical filter, the signal is handled in the Proportion Integration Differentiation controller. Finally, the electrical signal derived from the PID controller is applied to the PZT to finely tune the phase difference of the unbalanced interferometer. Remaining phase jitter comes from the slight misalignment between phase-locking light and signal photons, and note that the phase-locking light propagates around the loop once (for 3-m-long), while the signal photons propagate around three times (for 9-m-long), calling for more strict phase-locking robustness.

Here, the visibility V mainly depends on the cross correlation $g^{(2)}_{S-AS}$ between Stokes photons and anti-Stokes photons, and can be estimated by $V = (g^{(2)}_{S-AS} - 1)/(g^{(2)}_{S-AS} + 1)$[45,46]. In our experiment, the measured cross correlation is $g^{(2)}_{S-AS} = 15.39 \pm 0.26$, thus the estimated visibility is about 88%, which is almost equal to the values $(88 \pm 5)\%$ for N_+ and $(84 \pm 6)\%$ for N_- shown in Fig. 3. That implies the influence of the remaining phase drift on the visibility is not significant. In addition, since the control pulses and the phase locking light come from the same laser, the retrieved anti-Stokes photons and the phase-locking light experience a same frequency shift, thus the finite precision (about 5 MHz) of frequency locking process for the control light doesn't affect the stability of the interference between the two readout modes of anti-Stokes photons.

DATA AVAILABILITY

The data that support the findings of this study are available from the corresponding author on request.

Received: 22 April 2022; Accepted: 24 April 2023;
Published online: 26 June 2023

REFERENCES

1. Zarkeshian, P. et al. Entanglement between more than two hundred macroscopic atomic ensembles in a solid. *Nat. Commun.* **8**, 906 (2017).
2. Kotler, S. et al. Direct observation of deterministic macroscopic entanglement. *Science* **372**, 622–625 (2021).
3. Horodecki, R., Horodecki, P., Horodecki, M. & Horodecki, K. Quantum entanglement. *Rev. Mod. Phys.* **81**, 865–942 (2009).
4. Briegel, H. J., Dür, W., Cirac, J. I. & Zoller, P. Quantum repeaters: the role of imperfect local operations in quantum communication. *Phys. Rev. Lett.* **81**, 5932–5935 (1998).
5. Chou, C. W. et al. Functional quantum nodes for entanglement distribution over scalable quantum networks. *Science* **316**, 1316–1320 (2007).
6. Kimble, H. J. The quantum internet. *Nature* **453**, 1023–1030 (2008).
7. Chen, Y. A. et al. Memory-built-in quantum teleportation with photonic and atomic qubits. *Nat. Phys.* **4**, 103–107 (2008).
8. Giovannetti, G., Lloyd, S. & Maccone, L. Quantum-enhanced measurements: beating the standard quantum limit. *Science* **306**, 1330–1336 (2004).
9. Gottesman, D., Jennewein, T. & Croke, S. Longer-baseline telescopes using quantum repeaters. *Phys. Rev. Lett.* **109**, 070503 (2012).
10. Kómár, P. et al. A quantum network of clocks. *Nat. Phys.* **10**, 582–587 (2014).
11. Yin, J. et al. Satellite-based entanglement distribution over 1200 kilometers. *Science* **356**, 1140–1144 (2017).
12. Pang, X. L. et al. Experimental quantum-enhanced cryptographic remote control. *Sci. Rep.* **9**, 1–5 (2019).
13. Chou, C. W. et al. Measurement-induced entanglement for excitation stored in remote atomic ensembles. *Nature* **438**, 828–832 (2005).
14. Julsgaard, B., Kozhekin, A. & Polzik, E. S. Experimental long-lived entanglement of two macroscopic objects. *Nature* **413**, 400–403 (2001).
15. Yuan, Z. S. et al. Experimental demonstration of a BDCZ quantum repeater node. *Nature* **454**, 1098–1101 (2008).
16. Kong, J. et al. Measurement-induced, spatially-extended entanglement in a hot, strongly-interacting atomic system. *Nat. Commun.* **11**, 2415 (2020).
17. Li, H. et al. Multipartite entanglement of billions of motional atoms heralded by single photon. *npj Quantum Inf.* **7**, 146 (2021).
18. Hofmann, J. et al. Heralded entanglement between widely separated atoms. *Science* **337**, 72–75 (2012).
19. Moehring, D. L. et al. Entanglement of single-atom quantum bits at a distance. *Nature* **449**, 68–71 (2007).
20. Delteil, A. et al. Generation of heralded entanglement between distant hole spins. *Nat. Phys.* **12**, 218–223 (2016).
21. Klimov, P. V., Falk, A. L., Christle, D. J., Dobrovitski, V. V. & Awschalom, D. D. Quantum entanglement at ambient conditions in a macroscopic solid-state spin ensemble. *Sci. Adv.* **1**, e1501015 (2015).
22. Lee, K. C. et al. Entangling macroscopic diamonds at room temperature. *Science* **334**, 1253–1256 (2011).

23. Bernien, H. et al. Heralded entanglement between solid-state qubits separated by three metres. *Nature* **497**, 86–90 (2013).
24. Hensen, B. et al. Loophole-free Bell inequality violation using electron spins separated by 1.3 kilometres. *Nature* **526**, 682–686 (2015).
25. Humphreys, P. C. et al. Deterministic delivery of remote entanglement on a quantum network. *Nature* **558**, 268–273 (2018).
26. Ockeloen-Korppi, C. F. et al. Stabilized entanglement of massive mechanical oscillators. *Nature* **556**, 478–482 (2018).
27. Jin, X. M. et al. Experimental free-space quantum teleportation. *Nat. Photon.* **4**, 376–381 (2010).
28. Gisin, N. & Thew, R. Quantum communication. *Nat. Photon.* **1**, 165–171 (2007).
29. Ladd, T. D. et al. Quantum computers. *Nature* **464**, 45–53 (2010).
30. Aspuru-Guzik, A. & Walther, P. Photonic quantum simulators. *Nat. Phys.* **8**, 285–291 (2012).
31. Duan, L. M., Lukin, M. D., Cirac, J. I. & Zoller, P. Long distance quantum communication with atomic ensembles and linear optics. *Nature* **414**, 413–418 (2001).
32. Chaneliére, T. et al. Storage and retrieval of single photons transmitted between remote quantum memories. *Nature* **438**, 833–836 (2005).
33. Eisaman, M. D. et al. Electromagnetically induced transparency with tunable single-photon pulses. *Nature* **438**, 837–841 (2005).
34. Zhang, H. et al. Preparation and storage of frequency uncorrelated entangled photons from cavity-enhanced spontaneous parametric downconversion. *Nat. Photon.* **5**, 628–632 (2011).
35. Kuzmich, A. et al. Generation of nonclassical photon pairs for scalable quantum communication with atomic ensembles. *Nature* **423**, 731–734 (2003).
36. Chrapkiewicz, R., Dabrowski, M. & Wasilewski, W. High-capacity angularly multiplexed holographic memory operating at the single-photon level. *Phys. Rev. Lett.* **118**, 063603 (2017).
37. Hosseini, M., Sparkes, B. M., Campbell, G., Lam, P. K. & Buchler, B. C. High efficiency coherent optical memory with warm rubidium vapour. *Nat. Commun.* **2**, 174 (2011).
38. Liao, W. T., Keitel, C. H. & Pálffy, A. All-electromagnetic control of broadband quantum excitations using gradient photon echoes. *Phys. Rev. Lett.* **113**, 123602 (2014).
39. Julsgaard, B., Sherson, J., Cirac, J. I., Fiuŕašek, J. & Polzik, E. S. Experimental demonstration of quantum memory for light. *Nature* **432**, 482–486 (2004).
40. Reim, K. F. et al. Multi-pulse addressing of a Raman quantum memory: configurable beam splitting and efficient readout. *Phys. Rev. Lett.* **108**, 263602 (2012).
41. Ding, D. S. et al. Raman quantum memory of photonic polarized entanglement. *Nat. Photon.* **9**, 332–338 (2015).
42. Simon, C. et al. Quantum memories: a review based on the European integrated project "qubit applications (QAP)". *Eur. Phys. J. D* **58**, 1–22 (2010).
43. Pang, X. L. et al. A hybrid quantum memory enabled network at room temperature. *Sci. Adv.* **6**, eaax1425 (2020).
44. Clauser, J. F. Experimental distinction between the quantum and classical field-theoretic predictions for the photoelectric effect. *Phys. Rev. D* **9**, 853–860 (1974).
45. Bao, X. H. et al. Efficient and long-lived quantum memory with cold atoms inside a ring cavity. *Nat. Phys.* **8**, 517–521 (2012).
46. De Riedmatten, H. et al. Direct measurement of decoherence for entanglement between a photon and stored atomic excitation. *Phys. Rev. Lett.* **97**, 113603 (2006).
47. Dou, J. P. et al. A broadband DLCZ quantum memory in room-temperature atoms. *Commun. Phys.* **1**, 55 (2018).
48. Dou, J. P. et al. Direct observation of broadband nonclassical states in a room-temperature light-matter interface. *npj Quantum Inform.* **4**, 31 (2018).
49. Sangouard, N., Simon, C., De Riedmatten, H. & Gisin, N. Quantum repeaters based on atomic ensembles and linear optics. *Rev. Mod. Phys.* **83**, 33–80 (2011).
50. Berry, M. V. Quantal phase factors accompanying adiabatic changes. *Proc. R. Soc. Lond. A* **392**, 45–57 (1984).
51. Simon, J., Tanji, H., Ghosh, S. & Vuletić, V. Single-photon bus connecting spin-wave quantum memories. *Nat. Phys.* **3**, 765–769 (2007).
52. Laurat, J., Choi, K. S., Deng, H., Chou, C. W. & Kimble, H. J. Heralded entanglement between atomic ensembles: preparation, decoherence, and scaling. *Phys. Rev. Lett.* **99**, 180504 (2007).
53. Wootters, W. K. Entanglement of formation of an arbitrary state of two qubits. *Phys. Rev. Lett.* **80**, 2245 (1998).
54. Usmani, I. et al. Heralded quantum entanglement between two crystals. *Nat. Photon.* **6**, 234–237 (2008).
55. Zugenmaier, M., Dideriksen, K. B., Sørensen, A. S., Albrecht, B. & Polzik, E. S. Long-lived non-classical correlations towards quantum communication at room temperature. *Commun. Phys.* **1**, 76 (2018).
56. Dideriksen, K. B., Schmieg, R., Zugenmaier, M. & Polzik, E. S. Room-temperature single-photon source with near-millisecond built-in memory. *Nat. Commun.* **12**, 3699 (2021).
57. Katz, O., Shaham, R. & Firstenberg, O. Quantum interface for noble-gas spins based on spin-exchange collisions. *PRX Quantum* **3**, 010305 (2022).
58. Pang, X. L. et al. Supplementary materials for "A Hybrid quantum memory enabled network at room temperature". *Sci. Adv.* **6**, eaax1425 (2020).

ACKNOWLEDGEMENTS

The authors thank Jun Gao and Jian-Wei Pan for their helpful discussions. This research is supported by the National Key R&D Program of China (Grants No. 2019YFA0308700, No. 2019YFA0706302, and No. 2017YFA0303700); National Natural Science Foundation of China (NSFC) (Grants No. 62235012, No. 11904229, No. 12104299, No. 61734005, No. 11761141014, and No. 11690033); Science and Technology Commission of Shanghai Municipality (STCSM) (Grants No. 20JC1416300, and No. 2019SHZDZX01); Shanghai Municipal Education Commission (SMEC) (2017-01-07-00-02-E00049); China Postdoctoral Science Foundation (Grant No. 2020M671091, No. 2021M692094, No. 2022T150415); X.-M.J. acknowledges additional support from a Shanghai talent program and support from Zhiyuan Innovative Research Center of Shanghai Jiao Tong University.

AUTHOR CONTRIBUTIONS

X.-M.J. conceived and supervised the project. X.-L.P. and X.-M.J. designed the experiment. X.-L.P., C.-N.Z., J.-P.D., H.L., and T.-H.Y. performed the experiment. X.-L.P., C.-N.Z., J.-P.D., and X.-M.J. analyzed the data and wrote the paper. X.-L.P., C.-N.Z., and J.-P.D. contributed equally to this work.

COMPETING INTERESTS

The authors declare no competing interests.

ADDITIONAL INFORMATION

Correspondence and requests for materials should be addressed to Xian-Min Jin.